



Generalized Fresnel-Floquet equations for driven quantum materials

Marios H. Michael,^{1,2,*} Michael Först,² Daniele Nicoletti²,,² Sheikh Rubaiat Ul Haque,³ Yuan Zhang,³ Andrea Cavalleri,^{2,4} Richard D. Averitt,³ Daniel Podolsky⁵,,⁵ and Eugene Demler^{1,6}

¹*Department of Physics, Harvard University, Cambridge, Massachusetts 02138, USA*

²*Max Planck Institute for the Structure and Dynamics of Matter, Luruper Chausse 149, 22761 Hamburg, Germany*

³*Department of Physics, University of California San Diego, La Jolla, California 92093, USA*

⁴*Department of Physics, University of Oxford, Clarendon Laboratory, Parks Road, Oxford OX1 3PU, United Kingdom*

⁵*Department of Physics, Technion, 32000 Haifa, Israel*

⁶*Institute for Theoretical Physics, Wolfgang Pauli Str. 27, ETH Zurich, 8093 Zurich, Switzerland*



(Received 13 October 2021; revised 13 April 2022; accepted 15 April 2022; published 2 May 2022)

Optical drives at terahertz and midinfrared frequencies in quantum materials are increasingly used to reveal the nonlinear dynamics of collective modes in correlated many-body systems and their interplay with electromagnetic waves. Recent experiments demonstrated several surprising optical properties of transient states induced by driving, including the appearance of photo-induced edges in the reflectivity in cuprate superconductors (SCs), observed both below and above the equilibrium transition temperature. Furthermore, in other driven materials, reflection coefficients larger than unity have been observed. In this paper we demonstrate that unusual optical properties of photoexcited systems can be understood from the perspective of a Floquet system, a system with periodically modulated parameters originating from pump-induced oscillations of a collective mode. These oscillations lead to an effective Floquet system with periodically modulated parameters. We present a general phenomenological model of reflectivity from Floquet materials, which takes into account parametric generation of excitation pairs. We find a universal phase diagram of drive-induced features in reflectivity which evidence a competition between driving and dissipation. To illustrate our general analysis, we apply our formalism to two concrete examples motivated by recent experiments: A single plasmon band, which describes Josephson plasmons (JPs) in layered SCs, and a phonon-polariton system, which describes upper and lower polaritons in materials such as insulating SiC. Finally, we demonstrate that our model can be used to provide an accurate fit to results of phonon-pump-terahertz-probe experiments in the high-temperature SC $\text{YBa}_2\text{Cu}_3\text{O}_{6.5}$. Our model explains the appearance of a pump-induced edge, which is higher in energy than the equilibrium JP edge, even if the interlayer Josephson coupling is suppressed by the pump pulse.

DOI: [10.1103/PhysRevB.105.174301](https://doi.org/10.1103/PhysRevB.105.174301)

I. INTRODUCTION AND OVERVIEW

A. Motivation

Nonequilibrium dynamics in quantum materials is a rapidly developing area of research that lies at the interface between nonlinear optics and quantum many-body physics [1,2]. Indeed, a panoply of experimental results highlights the ability of ultrafast optical techniques to interrogate and manipulate emergent states in quantum materials. This includes photo-augmented superconductivity [3–6], unveiling hidden states in materials proximal to the boundary of an insulator-to-metal transition [7,8], and manipulating topological states [9–11]. The terahertz to midinfrared spectral range

is especially important as numerous phenomena in quantum materials manifest at these energies, including phonons, magnons, plasmons, and correlation gaps [12–14]. Access to this spectral range enables preferential pump excitation of specific degrees of freedom and probing of the resultant dynamics that are encoded in the dielectric response (and hence the reflectivity or transmission). Therefore a particular challenge is to decode the optical reflectivity dynamics which typically requires developing models that can be related to the underlying microscopic states. In short, it is crucial to develop a consistent framework for interpreting experimental results to aid in identifying emergent universal properties of driven states and to take full advantage of the plethora of “properties-on-demand” exhibited by quantum materials [12,15].

A common way of understanding pump and probe experiments has been based on the perspective of a dynamic trajectory in a complex energy landscape, where “snapshots” track the evolution of the slowly evolving but quasistationary many-body states [1,2,16]. Within this approach temporal evolution of spectroscopic features is interpreted using the conventional equilibrium formalism, and measured parameters serve as a fingerprint of the underlying instantaneous

*marios_michael@g.harvard.edu

Published by the American Physical Society under the terms of the [Creative Commons Attribution 4.0 International](https://creativecommons.org/licenses/by/4.0/) license. Further distribution of this work must maintain attribution to the author(s) and the published article's title, journal citation, and DOI. Open access publication funded by the Max Planck Society.

state. In particular, this approach has been applied to analyze c -axis terahertz reflectivity of the cuprate superconductors (SCs). In equilibrium, the Josephson plasma (JP) edge appears only below T_c indicating coherent c -axis Cooper-pair tunneling. Interband or phononic excitation along the c axis in several distinct cuprates (including $\text{La}_{1.675}\text{Eu}_{0.2}\text{Sr}_{0.125}\text{CuO}_4$, $\text{La}_{2-x}\text{Ba}_x\text{CuO}_4$, and $\text{YBa}_2\text{Cu}_3\text{O}_{6+\delta}$) resulted in the appearance of edgeline features in the terahertz c -axis reflectivity at temperatures above the equilibrium T_c [3–5,17]. These experiments were interpreted as providing spectroscopic evidence for light-induced modification of interlayer Josephson coupling. The central goal of this paper is to develop an alternative framework for interpreting optical responses of photoexcited materials. Our model focuses on features unique to nonequilibrium systems, in particular to photoexcited collective excitations which provide parametric driving of many-body systems. While we do not argue that this mechanism explains all experimental results on pump-induced changes in reflectivity, we believe that this scenario is sufficiently ubiquitous to merit detailed consideration. We provide universal expressions for driving induced changes in the reflectivity, which can be compared with experimental data, in order to examine the relevance of the parametric driving scenario to any specific experiment.

Before proceeding to discuss details of our model, it is worth reviewing several experiments that have already revealed pump-induced dynamics that cannot be interpreted from the perspective of equilibrium systems. Particularly striking are recent observations of light amplification of reflectivity in the photoexcited insulator SiC and the SC K_3C_{60} above its equilibrium T_c [18–20]. Furthermore, in the case of pumped $\text{YBa}_2\text{Cu}_3\text{O}_{6+\delta}$ discussed above, strong experimental evidence has accumulated indicating that an effective photo-induced edge arises from parametric amplification of Josephson plasmons (JPs) rather than a modification of the effective coupling [21,22] (see discussion in Sec. IV of this paper). Prior work also demonstrated higher harmonic generation from Higgs and other collective modes [23–25], nonlinear effects including parametric amplification of superconducting plasma waves [26–29], and time-resolved ARPES measurements of photoinduced Higgs oscillations in a charge-density wave [30]. A cursory understanding of these experiments can be obtained from the perspective of nonlinear optics deriving from coherent dynamics of order parameters and associated degrees of freedom such as phonons. However, several qualitative differences between collective mode optics and standard nonlinear optics deserve a special mention. First, in systems that we consider, a nonlinear response of the probe pulse persists at delay times well beyond the duration of the pump pulse. Hence one cannot apply theoretical approaches based on the expansion of optical nonlinearities in powers of the electric field, such as $\chi^{(2)}$, and $\chi^{(3)}$ [31]. Instead, it is imperative to analyze the interaction of the electromagnetic field of the probe pulse with matter degrees of freedom excited by the pump pulse. Second, it is important to properly account for the role of the surface, since the probe wavelength can be comparable or even larger than the penetration depth of the material. Thus common assumptions of nonlinear optics, including the slowly varying envelope approximation [31] and phase matching, need to be replaced by the explicit solution

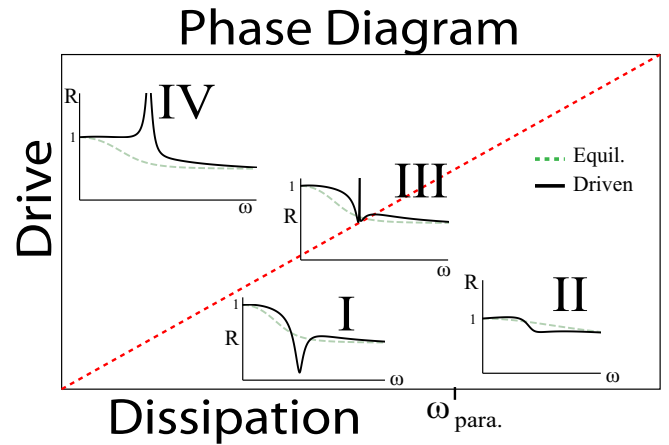


FIG. 1. Phase diagram of optical reflectivity of an interacting Floquet material as a function of the parametric drive amplitude and dissipation. We identify four regimes with qualitatively different types of reflectivity: (I) Weakly driven underdamped modes in the stable regime where dissipation, γ , is sufficient to prevent a lasing instability. The line shape is a square Lorentzian dip given by Eq. (1). (II) Weakly driven overdamped modes in the stable regime. The resonance feature is an edgeline shape given by Eq. (30). (III) Crossover regime on the boundary of the stable and unstable regions with a double dip structure. (IV) Unstable region, strong driving overcomes dissipation and may even lead to parametric amplification.

of Maxwell equations coupled to dynamical equations for matter.

B. Overview of results and organization of the paper

The primary goal of this paper is to present a general phenomenological formalism for discussing optical properties of driven states following a resonant excitation of a collective mode. We analyze the problem from the perspective of Floquet matter in which a collective mode excited by the pump provides temporal modulation of microscopic parameters of the material. This results in parametric driving of the system and Floquet-type mixing of frequencies. When the system is driven homogeneously in space (i.e., with wave-vector $k = 0$) and frequency Ω_d , a parametric resonance occurs whenever two collective excitations that are IR-active have the opposite wave vector, $k_1 = -k_2$, and frequencies that add up to the drive frequency, $\omega_1 + \omega_2 = \Omega_d$. Naively, one expects parametric resonances to always lead to enhancement of reflectivity, with sharp peaks corresponding to parametric resonance conditions [32,33]. We find that the situation is far richer and may include the appearance of edges, dips, and electromagnetically induced transparency (EIT)-type [34] structure in the reflectivity (see Fig. 1). Physically, this comes from oscillation-induced mixing between light-matter fields of different frequency components. In this paper, we focus on the case of oscillations with a small amplitude and/or strong dissipation, in which case analysis can be limited to the mixing of only two frequencies commonly referred to as the signal and idler frequencies. They are defined such that the signal frequency ω_s is equal to the frequency of the

probe pulse, whereas the idler frequency $\omega_{id.}$ is equal to the difference between the drive frequency Ω_d and ω_s . Interference between the signal and the idler frequency components is reminiscent of Fano-type phenomena in scattering theory and optics, where interference between two channels can result in nontrivial energy dependence of the reflection and transmission coefficients [35]. Describing the driving only in terms of signal and idler mixing corresponds to a degenerate perturbation theory in the Floquet basis [20,36,37].

What determines whether interference phenomena will dominate over parametric amplification of reflectivity is the competition between parametric driving and losses. We find a universal dynamical phase diagram of the optical response as a function of the strength of the drive and dissipation. Remarkably, we find that the entire breadth of these responses can be specified using only a few effective (phenomenological) parameters. One of the main achievements of this paper is to derive analytical formulas for the shape of these resonances in Sec. II C in the case of strong dissipation where perturbation theory is valid; see Regimes I and II in Fig. 1. In Regime I, corresponding to the case of underdamped collective modes, we obtain a Lorentzian square shape:

$$R_{\text{driven}} = R_s \left(1 + \alpha \text{Re} \left\{ \frac{1}{(\omega - \omega_{\text{para.}} + i\gamma)^2} \right\} \right), \quad (1)$$

where R_{driven} is the reflectivity in the Floquet state, R_s is the reflectivity in equilibrium, α is a frequency-dependent parameter that depends on dispersion of the IR collective modes of the material, $\omega_{\text{para.}}$ is the frequency at which parametric resonance condition is satisfied, and γ the dissipation in the system. Notably, in Regime I, we can use the Floquet drive to directly extract the dissipation in the system on parametric resonance. In Regime II, corresponding to overdamped collective modes, the resonance peak has the form

$$R_{\text{driven}} = R_s \left(1 + \beta \text{Re} \left\{ e^{i\theta} \frac{1}{\omega - \omega_{\text{para.}} + i\gamma} \right\} \right), \quad (2)$$

where β and θ are frequency-dependent parameters that depend on the dispersion of IR collective modes. In this case, the shape is a linear combination of a real and imaginary Lorentzian function resulting in an effective “edge”-like feature.

For clarity, in this work we simplify our analysis by including Floquet modulation at a single frequency. When the finite lifetime of the collective mode is taken into account, this should be analyzed as a multitonal drive. Our analysis can be generalized to this situation. However, in the current paper we will only comment on the main changes that we expect in this case. We postpone a detailed discussion of the multitonal Floquet-Fresnel problem to a future publication [38].

It is worth noting conceptual connections between our Floquet approach and previous work on the phenomenon of optical phase conjugation (OPC) [39,40]. What makes our analysis different is that we focus on terahertz phenomena, which correspond to much longer wavelengths than optical phenomena considered in the context of OPC. It is important for our discussion to take into account that nonlinear processes take place near the material boundary rather than in the bulk, which is why our starting point is the Fresnel formalism of

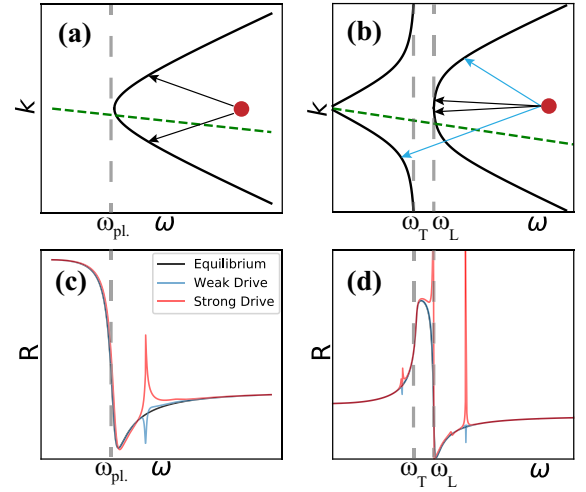


FIG. 2. Examples of dispersion relations (a), (b) and their corresponding reflectivity spectrum (c), (d). (a) Dispersion relation of a plasmon in a SC (black) and dispersion relation of light in air (green). The corresponding equilibrium reflectivity in (c) shows perfect reflection below the gap for $\omega_s < \omega_{\text{pl.}}$, and a minimum in reflectivity appears when the dispersion of light in air crosses the dispersion of the plasmon in the material, a condition called phase matching. (b) Dispersion relation of phonon-polariton (black) and dispersion relation of light in air (green). The corresponding equilibrium reflectivity in (d) shows perfect reflectivity inside the *reststrahlen band* and plasma edge when the dispersion of light in air crosses the dispersion of the upper polariton similarly to (c). The red dots in (a) and (b) show the driving frequency, while the arrows depict the parametrically resonant processes resulting from the Floquet drive. This leads to features in the reflectivity predicted by our theory at the parametrically resonant frequencies both for strong and for weak drive relative to dissipation.

reflection of electromagnetic waves. This can be contrasted to phase-matching conditions used in most discussions of OPC, which essentially assume that nonlinear processes take place in the bulk of the material.

This paper is organized as follows. Section II presents a general formalism for computing the reflectivity of Floquet materials. With a goal of setting up notation in Sec. II A, we remind the readers regarding the canonical formalism of Fresnel’s solution of light reflection from an equilibrium material with an index of refraction $n(\omega)$. In Sec. II B we discuss how to generalize this approach to study light reflection from a material subject to a periodic drive. We show a universal form of frequency dependence of reflectivity from such systems, which we summarize in the phase diagram presented in Fig. 1. We show that this frequency dependence can be deduced from the dispersion of collective modes and frequency of the periodic drive without developing a full microscopic theory. Thus the Floquet-Fresnel equations allow for the same level of conceptual understanding as the standard equilibrium Fresnel problem. To make our discussion more concrete, in Sec. III we apply this analysis to two paradigmatic cases: (i) A single low-frequency plasmon band and (ii) the two band case of a phonon-polariton system with dispersions shown in Fig. 2. These two cases are not only exemplary but also provide accurate models for real materials, such as the lower JP of

YBa₂Cu₃O_{6+x} [case (i)] and a phonon-polariton system in SiC [case (ii)]. They are reviewed in Secs. III A and III B, respectively. We note that most cases of parametric resonance in pump and probe experiments can be reduced to these two examples, since the usual formulation of parametric resonance involves generating pairs of excitations and the resonance can be described by including up to two bands. However, in some cases there may be additional features in the reflectivity arising from the singular behavior of matrix elements. We provide a concrete example of this in Sec. III B for the case of phonon-polariton model in SiC. Finally, we demonstrate that our theory enables a quantitatively accurate fit to the results of pump and probe experiments in YBa₂Cu₃O_{6.5}. These experiments demonstrated the appearance of a photo-induced edge both below and above the superconducting transition temperature at frequencies close to the lower plasmon edge. We demonstrate that these observations can be accurately described by the Floquet-Fresnel model developed in this paper.

II. GENERAL FORMALISM OF FLOQUET-FRESNEL REFLECTION

A. Equilibrium reflectivity

We begin our discussion by presenting coupled dynamical equations for light and matter, assuming that the material has an infrared active collective mode, such as a phonon or a JP. Information about the collective mode is included in the frequency dependence of the linear electric susceptibility, $\chi(\omega, k)$, which determines the index of refraction $n(\omega)$:

$$\nabla \times B = \mu_0 \partial_t D, \quad (3a)$$

$$\nabla \times E = -\partial_t B, \quad (3b)$$

$$D = \epsilon_0 E + P, \quad (3c)$$

where the dynamics of the polarization P contain all optically active collective modes inside the material, E is the electric field, and ϵ_0 and μ_0 are the electric permittivity and magnetic permeability in vacuum, respectively. The polarization in frequency and momentum space, $P(\omega, k)$, is given in terms of the electric field through the linear susceptibility, $P(\omega, k) = \epsilon_0 \chi(\omega, k) E(\omega, k)$. Due to the high speed of light, c , considerable hybridization between the collective mode and light occurs only at very small momenta, $k \sim \frac{\omega}{c}$. As a result, for optical reflection problems we can take the susceptibility to be dispersionless, $\chi(\omega, k) \approx \chi(\omega, k=0) \equiv \chi(\omega)$ to a good approximation. Combining the Maxwell equations with the susceptibility we find the dynamics of the electromagnetic transverse modes in frequency and momentum space to be given by a wave equation with a solely frequency-dependent refractive index $n(\omega)$:

$$\left(\frac{n^2(\omega)\omega^2}{c^2} - k^2 \right) E(\omega, k) = 0. \quad (4)$$

Collective mode dispersion relations are found as solutions to the equation $(k^2 - \frac{\omega^2 n^2(\omega)}{c^2}) = 0$. The above description is very general and any dispersion relation inside the material can be captured by an appropriate choice of $n(\omega)$.

1. The case of a plasmon

In SCs the Anderson-Higgs mechanism gives rise to the gap in the spectrum of transverse electromagnetic fields equal to the plasma frequency; see Fig. 2(a). The plasmon excitation can be captured by a refractive index of the type [41]:

$$n_{SC}^2(\omega) = \epsilon_\infty \left(1 - \frac{\omega_{pl.}^2}{\omega^2} \right), \quad (5)$$

where $\omega_{pl.}$ is the plasma frequency and ϵ_∞ is a constant background permittivity. Such a refractive index when substituted in Eq. (4) leads to the dispersion relation for the electromagnetic field inside a SC to be:

$$\omega_{SC}^2(k) = \omega_{pl.}^2 + \frac{c^2}{\epsilon_\infty} k^2. \quad (6)$$

We note that plasmon modes can have very different frequencies depending on light polarization. In particular, in the case of layered systems, such as YBa₂Cu₃O_{6+x} SCs, the plasma frequency is small for electric-field polarization perpendicular to the layers. In layered metals one can also find low-energy plasmon modes, although they typically have stronger damping than in SCs.

2. Phonon-polariton systems

Another ubiquitous example is the case of phonon-polaritons. In this paper we will primarily use SiC for illustration, which features an IR-active phonon at frequency close to 30 THz with a large effective charge [18]. Another related material that is currently under active investigation is Ta₂NiSe₅, which has an additional complication that multiple phonons need to be included in the analysis.

In the case of a single IR phonon the dispersion relation of the phonon-polariton system is depicted in Fig. 2(b). It can be captured by substituting in Eq. (4) the refractive index [37]:

$$n_{\text{phonon}}^2(\omega) = \epsilon_\infty \left(1 - \frac{\omega_{pl.,\text{phonon}}^2}{\omega^2 + i\gamma\omega - \omega_{ph.}^2} \right), \quad (7)$$

where $\omega_{pl.,\text{phonon}}$ is the plasma frequency of the phonon mode, $\omega_{ph.}$ is the transverse phonon frequency, and γ is a dissipative term for the phonon.

3. The case of multiple IR modes

In the case when multiple IR-active collective modes need to be included in the analysis (phonons, plasmons, etc.), it is common to use the Lorentz model which parametrizes the contribution of each collective mode to the refractive index by a Lorentzian [42]:

$$n^2(\omega) = \epsilon_\infty \left(1 - \sum_i \frac{\omega_{pl.,i}^2}{\omega^2 + i\gamma_i\omega - \omega_i^2} \right), \quad (8)$$

where ω_i is the bare frequency of the i th collective mode, $\omega_{pl.,i}$ is the plasma frequency which characterizes the strength of the coupling to light, γ_i is the dissipation, and ϵ_∞ is an effective static component to the permittivity arising from high-energy modes not included in the sum. The above discussion illustrates that Eq. (4) is very general, and in any case

an appropriate $n(\omega)$ can be chosen to capture the dispersion relation of optically active bands.

4. Fresnel equations

We begin by reviewing the Fresnel light reflection problem at the interface between air and material in equilibrium. While this is textbook material, we present it here with the goal of establishing notations for subsequent discussion of the nonequilibrium case. We consider an incoming beam with frequency ω_s at normal angle of incidence

$$E_s = E_0 e^{i \frac{\omega_s}{c} z - i \omega_s t}, \quad (9)$$

where z is the direction perpendicular to the interface and the interface lies at $z = 0$. The reflected and transmitted waves at the signal frequency are expressed through reflection and transmission coefficients, $E_r = r_s E_0 e^{-i \frac{\omega_s}{c} z - i \omega_s t}$ and $E_t = t_s E_0 e^{i k_s z - i \omega_s t}$. The momentum k_s corresponds to the mode inside the material oscillating at ω_s and using Eq. (4) is given by $k_s = \frac{\omega_s n(\omega_s)}{c}$. Matching the electric field across the boundary at $z = 0$ gives rise to the boundary equation:

$$1 + r_s = t_s. \quad (10)$$

For nonmagnetic materials, the magnetic field is also conserved across the surface. Using the homogeneous Maxwell equation, $\partial_t B = -\nabla \times E$, we calculate the magnetic field in the two regions. Matching the two regions at $z = 0$ gives rise to the second boundary equation:

$$1 - r_s = n(\omega_s) t_s. \quad (11)$$

Solving for the reflection coefficient, we find the standard expression for reflectivity in terms of the refractive index:

$$R_s = |r_s|^2 = \left| \frac{1 - n(\omega_s)}{1 + n(\omega_s)} \right|^2 = \frac{(1 - n')^2 + (n'')^2}{(1 + n')^2 + (n'')^2}, \quad (12)$$

where n' and n'' correspond to the real and imaginary parts of the refractive index, respectively.

In equilibrium, reflectivity can be deduced, at least qualitatively, from the form of collective mode dispersion inside the material. This is depicted in Figs. 2(a)–2(c) for a SC and in Figs. 2(b)–2(d) for a photon-polariton system. In the case of a SC, at probing frequencies below the plasma gap $\omega_s < \omega_{pl}$, no bulk modes exist to propagate the energy and k_s is purely imaginary corresponding to an evanescent wave. In this situation, we have near perfect reflectivity. As soon as the probing frequency becomes larger than the plasma gap, transmission is allowed and reflectivity drops abruptly, reaching a minimum at the frequency where the light cone crosses the plasma band. The minimum in reflectivity or equivalently the maximum in transmission occurs when the incoming and transmitted waves are “phase matched,” a condition that is satisfied when the light cone in air crosses a new band inside the material, i.e., $n'(\omega_s) = 1$ in Eq. (12). The sudden drop in reflectivity appearing whenever a new optically active band becomes available is called in the literature a “plasma edge.” Similar reasoning can be used to determine qualitatively the reflectivity of a phonon-polariton system from its dispersion relation alone: At frequencies within the gap of the dispersion, $\omega_{ph.} < \omega_s < \sqrt{\omega_{ph.}^2 + \omega_{pl.,phonon}^2}$, called the *reststrahlen*

band, only evanescent waves are allowed, and reflectivity is expected to be close to one. On the other hand, for probing frequencies $\omega_s > \sqrt{\omega_{ph.}^2 + \omega_{pl.}^2}$, when the light cone crosses the upper polariton branch, a plasma edge appears.

5. Dissipation

Finally, we comment on the effects of dissipation on light reflection. While in principle Eq. (4) is completely general, it is sometimes helpful to add dissipation explicitly through the conductivity of the normal electron fluid which obeys Ohm’s law and modifies Eq. (4) to

$$\left(n^2(\omega) \omega^2 + i \frac{\sigma_n}{\epsilon_0} \omega - c^2 k^2 \right) E = 0, \quad (13)$$

where σ_n is the normal electron fluid conductivity. Such a term provides a natural way of including increased dissipation in the pumped state discussed below as a result of the presence of photo-excited carriers. In the equilibrium case, dissipation acts to smooth out sharp features in reflectivity such as the plasma edges.

B. Floquet reflectivity

1. Floquet eigenstates

Our goal in this section is to introduce a simple model for Floquet materials and discuss special features in reflectivity that appear in this model close to parametric resonances. In the next section we will demonstrate that features discussed in this section are ubiquitous and can be found in more accurate models [22,37]. We model the Floquet medium by assuming that the presence of an oscillating field inside the material results in a time periodic refractive index, $n_{\text{driven}}^2(t) = n^2(\omega) + \delta n_{\text{drive}}^2 \cos(\Omega_d t)$. In this simple model, the origin of the oscillating refractive index is the modulation left in the material after photo excitation of a certain collective mode; hence its lifetime can exceed the duration of the driving field. The equations of motion in frequency space for the electric field in the presence of the time-dependent perturbation becomes:

$$\left(k^2 - \frac{\omega^2 n^2(\omega)}{c^2} \right) E(\omega, k) + A_{\text{drive}} (E(\omega - \Omega_d, k) + E(\omega + \Omega_d, k)) = 0, \quad (14)$$

where A_{drive} is the mode coupling strength related to the amplitude of the time-dependent drive, which in this section we assume to be constant although, in principle, it may be frequency dependent (see, e.g., Sec. III B). Generally, equations of the type (14) should be solved simultaneously for many frequency components that differ by integer multiples of the drive frequency. However, to capture parametric resonances in the spectrum, it is sufficient to limit analysis to mixing between only two modes, which are commonly referred to as the signal and idler modes [43]. The signal frequency is taken to be the frequency of the probe pulse, whereas the idler frequency is chosen from the condition that the sum of the signal and idler frequency is equal to the drive frequency. There may be other resonant Floquet conditions, such as $\omega_1 - \omega_2 = \Omega_d$, which do not correspond to parametric

generation of excitations by the drive but instead correspond to resonant rescattering. We postpone discussion of such cases to subsequent publications. Thus we consider

$$E(t, z) = (E_s e^{-i\omega_s t} + E_{id}^* e^{+i\omega_{id} t}) e^{ikz}. \quad (15)$$

Truncating the eigenmode ansatz to only signal and idler components corresponds to using Floquet degenerate perturbation theory approximation [36]. The inclusion of higher harmonic contributions will give rise to subleading perturbative corrections. With the ansatz in Eq. (15), the equations of motion take the form:

$$\begin{pmatrix} k_s^2 - k_s^2 & A_{\text{drive}} \\ A_{\text{drive}} & k_{id}^2 - k_{id}^2 \end{pmatrix} \cdot \begin{pmatrix} E_s \\ E_{id}^* \end{pmatrix} = 0, \quad (16)$$

where $k_s^2(\omega_s) = \frac{\omega_s^2 n^2(\omega_s)}{c^2}$ and $k_{id}^2(\omega_{id}) = \frac{\omega_{id}^2 n^2(\omega_{id})}{c^2}$ are the momentum of the eigenstate oscillating at the signal frequency or idler frequency, respectively, in the absence of the parametric drive A_{drive} . The renormalized eigenvalues are given by:

$$k_{\pm}^2 = \frac{k_s^2 + k_{id}^2}{2} \pm \sqrt{\left(\frac{k_s^2 - k_{id}^2}{2}\right)^2 + A_{\text{drive}}^2}, \quad (17a)$$

and the corresponding Floquet eigenstates are:

$$E_{id, \pm}^* = \alpha_{\pm} E_{s, \pm}, \quad (18a)$$

$$\alpha_{\pm} = \frac{k_s^2 - k_{id}^2}{2A_{\text{drive}}} \mp \sqrt{\left(\frac{k_s^2 - k_{id}^2}{2A_{\text{drive}}}\right)^2 + 1}. \quad (18b)$$

2. Floquet-Fresnel equations

The eigenstates in Eq. (18) represent two transmission channels for the case where the Floquet material is probed at the signal frequency, $E_{\pm}(t, z) = t_{\pm} E_0 (e^{-i\omega_s t} + \alpha_{\pm} e^{+i\omega_{id} t}) e^{ik_{\pm} z}$. Similarly, the transmitted magnetic field is given by $B_{\pm}(t, z) = k_{\pm} t_{\pm} E_0 (\frac{1}{\omega_s} e^{-i\omega_s t} - \frac{\alpha_{\pm}}{\omega_{id}} e^{+i\omega_{id} t}) e^{ik_{\pm} z}$. To find the reflectivity, we need to satisfy boundary conditions corresponding to matching of magnetic and electric fields across the boundary oscillating at the signal and idler frequency separately:

$$1 + r_s = t_+ + t_-, \quad (19a)$$

$$1 - r_s = \frac{ck_+}{\omega_s} t_+ + \frac{ck_-}{\omega_s} t_-, \quad (19b)$$

$$r_{id} = \alpha_+ t_+ + \alpha_- t_-, \quad (19c)$$

$$r_{id} = \frac{ck_+}{\omega_{id}} \alpha_+ t_+ + \frac{ck_-}{\omega_{id}} \alpha_- t_-, \quad (19d)$$

where r_{id} is the coefficient of the light reflected at the idler frequency. The Fresnel-Floquet problem in Eq. (19) together with Eqs. (17) and (18) form a closed set of equations that can be solved to determine the reflectivity $R = |r_s|^2$.

3. Perturbation theory for large dissipation

In order to elucidate the physics of photo-induced resonances, it is instructive to work perturbatively in the parametric driving strength, away from parametric resonance. Since $k_s = k_{id}$ corresponds to the parametric resonance condition, the small parameter is chosen to be $\xi = \frac{2A_{\text{drive}}}{k_s^2 - k_{id}^2}$. In the limit of small ξ , the two solutions can be safely separated into

a mostly signal solution and a mostly idler solution. These correspond to expansions of k_{\pm}^2 to linear order in ξ

$$\tilde{k}_s^2 \approx k_s^2 + \frac{A_{\text{drive}} \xi}{2} + \mathcal{O}(A_{\text{drive}} \xi^3), \quad (20a)$$

$$\tilde{k}_{id}^2 \approx k_{id}^2 - \frac{A_{\text{drive}} \xi}{2} + \mathcal{O}(A_{\text{drive}} \xi^3), \quad (20b)$$

where \tilde{k}_s and \tilde{k}_{id} are the renormalized momenta. The corresponding transmission channels are given by expanding α_{\pm} to leading order in ξ :

$$E_1 = t_s E_0 \left(e^{-i\omega_s t} - \left(\frac{\xi}{2} + \mathcal{O}(\xi^3) \right) e^{+i\omega_{id} t} \right) e^{i\tilde{k}_s z} \quad (21a)$$

$$E_2 = t_{id} E_0 \left(\left(\frac{\xi}{2} + \mathcal{O}(\xi^3) \right) e^{-i\omega_s t} + e^{+i\omega_{id} t} \right) e^{i\tilde{k}_{id} z}, \quad (21b)$$

where the eigenmodes have been rescaled in perturbation theory in order to interpret E_1 as the channel oscillating primarily at the signal frequency with a perturbative mixing of the term oscillating at the idler frequency, while E_2 is the channel oscillating primarily at the idler frequency with a perturbative mixing of a term oscillating at the signal frequency. By integrating out the idler transmission channel, the Floquet-Fresnel equations can be reformulated through an effective renormalized refractive index (see Appendix A for details):

$$1 + r_s = t_s, \quad (22a)$$

$$1 - r_s = t_s \tilde{n}, \quad (22b)$$

where \tilde{n} is given by:

$$\tilde{n} = n_{eq} \left(1 + \frac{A_{\text{drive}} \xi}{4k_s^2} + \frac{\xi^2}{4} \frac{c\tilde{k}_s - \omega_{id}}{c\tilde{k}_{id} - \omega_{id}} \left(\frac{\tilde{k}_{id}}{\tilde{k}_s} - 1 \right) \right), \quad (23)$$

where n_{eq} is the equilibrium refractive index. Unlike equilibrium, the dressed Floquet refractive index is allowed to be negative giving rise to parametric amplification of the reflected signal. Equation (23) has two perturbative corrections to second order in the mode coupling strength's amplitude, A_{drive} : One of order ξ and the other of order ξ^2 . The term linear in ξ comes from the renormalization of the transmitted wave-vector \tilde{k}_s , while the quadratic term results from integrating out the idler channel and therefore originates from interference effects between signal and idler mode.

On parametric resonance within the same band, the phase-matching condition between signal and idler $|\text{Re}(k_s)| = |\text{Re}(k_{id})|$, implies $\omega_s = \omega_{id} = \frac{\xi \omega_d}{2}$, while the sign of each wave vector is fixed by causality as we show below. The perturbation theory developed above is valid even on resonance provided that the dissipation is high enough. To show this we expand around the parametrically resonant frequency, $\omega_s = \omega_{\text{para}}$, with a finite dissipation that we include in a causal way through the substitution $\omega_s \rightarrow \omega_s + i\gamma$. The expressions for the signal and idler wave vectors are then given by:

$$k_s = k'_{s,0} + \frac{\omega_s - \omega_{\text{para}} + i\gamma}{v_g(\omega_{\text{para}})}, \quad (24a)$$

$$k_{id} = -k'_{s,0} + \frac{\omega_s - \omega_{\text{para}} + i\gamma}{v_g(\omega_{\text{para}})}. \quad (24b)$$

In Eq. (24), $v_g(\omega_{\text{para}})$ is the group velocity on parametric resonance, and $k'_{s,0}$ the real part of the k_s wave vector on

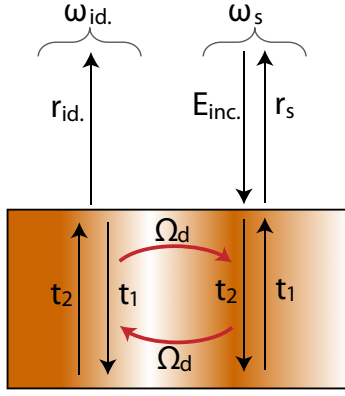


FIG. 3. Schematic depiction of counterpropagating transmission channels inside a Floquet material. In the presence of a Floquet drive, signal and idler frequency components are mixed giving rise to two transmission channels, t_1 and t_2 , propagating in opposite directions. Since the idler component is counteroscillating compared with the signal, the Floquet drive, which mixes signal and idler effectively, acts as a wall reflecting each transmission channel and changing its propagation direction. The two channels are coupled at the interface through the boundary conditions. The picture explains schematically the physical mechanism of parametric amplification: In the presence of a drive, solutions of the Fresnel equations exist which propagate from inside the material toward the surface, amplifying the reflectivity.

parametric resonance. Boundary conditions require that the transmitted light vanishes at large distances inside the material or equivalently $\text{Im}\{k\} > 0$. As a result, the real part of $k_{id.}$ is negative and counterpropagates with respect to the mostly signal transmission channel inside the material. This situation is shown schematically in Fig. 3. Using Eq. (24), the parameter ξ is given by

$$\xi \approx \frac{A_{\text{drive}}}{2(\omega_s - \omega_{\text{para}} + i\gamma) \frac{k'_{s,0}}{v_g(\omega_{\text{para}})}} \quad (25)$$

and has a Lorentzian peak structure. The resonant form of ξ is responsible for resonances in the reflectivity. In the case of multiple bands, the above result can be generalized by considering that the phase-matching condition between signal and idler wave can occur at different signal and idler frequencies $\omega_{\text{para},1} + \omega_{\text{para},2} = \Omega_d$. In this situation we have:

$$k_s = k'_{s,0} + \frac{\omega_s - \omega_{\text{para},1} + i\gamma(\omega_{\text{para},1})}{v_g(\omega_{\text{para},1})}, \quad (26a)$$

$$k_{id.} = -k'_{s,0} + \frac{\omega_{id.} - \omega_{\text{para},1} + i\gamma(\omega_{\text{para},2})}{v_g(\omega_{\text{para},2})}, \quad (26b)$$

where the group velocity and dissipation can be different for the different bands at $\omega_{\text{para},1}$ and $\omega_{\text{para},2}$. However, the perturbative parameter ξ for multiple bands takes a form similar to the single band case:

$$\xi = \frac{2A_{\text{drive}}}{k_s^2 - (k_{id.})^2} \approx \frac{A_{\text{drive}}}{2(\omega_s - \omega_{\text{para},1} + i\gamma_{\text{eff}}) \times \frac{k'_{s,0}}{v_{\text{eff}}}} \quad (27)$$

where $2v_{\text{eff}}^{-1} = v_g^{-1}(\omega_{\text{para},1}) + v_g^{-1}(\omega_{\text{para},2})$ and $\gamma_{\text{eff}} = \frac{\gamma_{\text{eff}}}{2} \cdot (\frac{\gamma(\omega_{\text{para},1})}{v_g(\omega_{\text{para},1})} + \frac{\gamma(\omega_{\text{para},2})}{v_g(\omega_{\text{para},2})})$. Equation (27) demonstrates that for

small driving strength the resonant behavior of parametric driving within the same band and in between different bands is the same.

C. Floquet-Fresnel phase diagram

Based on our analysis, resonant features in the reflectivity can be classified into four regimes as shown in Fig. 1. Regimes I and II are in the stable region where dissipation is stronger than the parametric drive. For these cases we can obtain analytic expressions for the changes in reflectivity. To second order in A_{drive} we find two contributions to the refractive index given in Eq. (23). Band renormalization gives rise to a linear contribution in ξ , while interference between signal and idler gives rise to a term proportional to ξ^2 . Their relative strength is given by $\frac{\delta n_{\text{linear}}}{\delta n_{\text{quadratic}}} \propto \frac{\gamma}{v_g k_s}$ on parametric resonance, $|Re(k_s)| = |Re(k_{id.})|$, c.f. Eq. (23). Interference phenomena dominate for underdamped photon modes for which $\gamma < v_g k_s$ while for overdamped modes interference phenomena are suppressed and band renormalization is dominant. The corresponding changes to reflectivity are calculated by expanding the reflectivity to linear order in δn

$$\tilde{n} = n_{eq.} + \delta n, \quad (28a)$$

$$\tilde{r}_s = \frac{1 - \tilde{n}}{1 + \tilde{n}} \approx r_{s,eq.} - \frac{2\delta n}{(n+1)^2}, \quad (28b)$$

$$\tilde{R}_s \approx R_{s,eq.} - 4\text{Re}\left\{\frac{\delta n}{(n+1)^2} r_s^*\right\}. \quad (28c)$$

1. Regime I

For the usual case of underdamped modes and a single band, we can take $r_{s,eq.}$ and $n_{eq.}$ to be real. Moreover, the constant, $A = \frac{c\tilde{k}_s - \omega_{id.}}{-c\tilde{k}_{id.} + \omega_{id.}}(1 + \frac{-\tilde{k}_{id.}}{\tilde{k}_s})$, can be expanded around parametric resonance to give $A = 2\frac{n-1}{n+1} = 2r_s$. Under these assumptions, interference of signal and idler gives rise to a double Lorentzian dip in reflectivity and is reminiscent of EIT.

$$\tilde{R}_s \approx R_{s,eq.} \left(1 - \frac{2}{(n+1)^2} \text{Re}\left\{\frac{C}{(\omega_s - \omega_{s,para} + i\gamma)^2}\right\}\right), \quad (29)$$

where $C = \frac{v_g^2 A_{\text{drive}}^2}{4k_s^2}$ is a constant proportional to the driving intensity.

2. Regime II

In the opposite limit of overdamped dynamics in a single band, the dominant term comes from the linear in ξ term and the reflectivity takes the form:

$$\tilde{R}_s \approx R_{s,eq.} + C' \text{Re}\left\{e^{i\theta} \frac{1}{\omega_s - \omega_{s,para} + i\gamma}\right\}, \quad (30)$$

where $C' e^{i\theta} = -\frac{1}{(n+1)^2} \frac{A_{\text{drive}}^2 v_g^2}{4k_s^3}$. This feature appears as a plasma edge induced by the drive from a featureless overdamped background as reported in Ref. [21].

3. Regimes III and IV

These regimes are not perturbative; however, in many cases we can use our simple theory of parametric resonance between

two bands to capture the reflectivity of real experiments by solving Eqs. (19a)–(19d). In particular, Regime IV corresponds to a lasing instability regime where we expect a strong peak in the reflectivity due to parametric amplification and can even be a discontinuous function (as it was also shown in Ref. [37]). Regime III is an intermediate region where on resonance there is amplification. However, away from resonance perturbation theory still holds giving rise to an interesting double dip structure.

III. EXAMPLES OF MANIFESTATIONS OF PARAMETRIC RESONANCE IN REFLECTIVITY

In the previous section, we investigated general aspects of Floquet resonances while being agnostic about microscopic details of the system. In this section, we discuss toy models of realistic dispersion. Pump-induced features in these toy models in the different regimes of the pump-induced phase diagram can be used to build intuition for more complicated multiband dispersions.

A. Driven plasmon band

The simplest case of an optical system that we discuss is a single plasmon band, which describes electrodynamics of metals and SCs. The equilibrium reflectivity in such systems was discussed in Sec. II A. Maxwell's equations in a SC can be written as [41]:

$$\left(\omega^2 - \omega_{pl}^2 + i\frac{\sigma_n}{\epsilon_0}\omega - c^2k^2\right)E = 0, \quad (31)$$

where σ_n represents the ohmic part of the conductivity and provides dissipation, while the photon obtains a mass given by the plasma frequency. At $\omega = 0$ Eq. (31) can be solved with $k = i\omega_p$, which corresponds to the skin effect in metals and for SCs can also be understood as the Meissner effect. The dissipation term with σ_n in Eq. (31) can be present in SCs due to quasiparticles [44]. The above equations of motion can be represented by the complex refractive index:

$$n_{SC}(\omega) = \frac{\omega^2 - \omega_{pl}^2}{\omega^2} + \frac{i\sigma_n}{\epsilon_0\omega}. \quad (32)$$

We model the Floquet material as a system with time-periodic modulation of the plasma frequency ω_{pl} at frequency Ω_d . We assume that the modulation frequency is higher than twice the frequency of the bottom of the plasmon band, so that the drive can result in resonant generation of plasmon pairs. Taking the amplitude of modulation to be A_{drive} we obtain Eq. (14) introduced previously.

Reflectivity spectra in the different regimes of the parametric driving-induced phase diagram are plotted in Fig. 4 by tuning the dissipation through the normal conductivity σ_n and the amplitude of periodic oscillations A_{drive} .

B. Floquet-Fresnel reflectivity in a phonon-polariton system

We now want to demonstrate that the four regimes presented in Fig. 1 are universal and not limited to a single optical band model. To this end we consider a system that features two branches of optical excitations: A phonon-polariton system corresponding to light coupling to a single IR-active

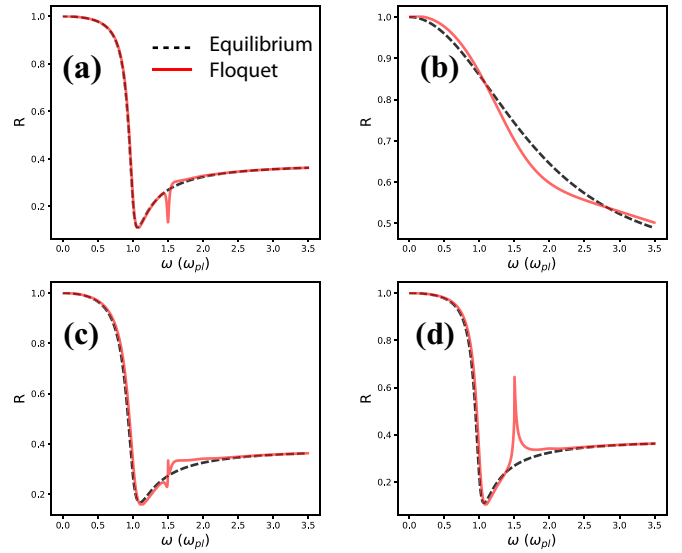


FIG. 4. Reflectivity spectra of a plasmon band driven at $\Omega_d = 3\omega_{pl}$ in the four different regimes of the phase diagram of Fig. 1. (a) Regime I: $\frac{\sigma_n}{\epsilon_0} = 0.064\omega_{pl}$, $A_{ampl.} = 3\frac{\omega_{pl}^2}{c^2}$; (b) Regime II: $\frac{\sigma_n}{\epsilon_0} = 2\omega_{pl}$, $A_{ampl.} = 60\frac{\omega_{pl}^2}{c^2}$; (c) Regime III: $\frac{\sigma_n}{\epsilon_0} = 0.1\omega_{pl}$, $A_{ampl.} = 6\frac{\omega_{pl}^2}{c^2}$; (d) Regime IV: $\frac{\sigma_n}{\epsilon_0} = 0.064\omega_{pl}$, $A_{ampl.} = 6\frac{\omega_{pl}^2}{c^2}$. Notice that dissipation suppresses parametric driving effects and a larger oscillation amplitude is needed to produce an appreciable effect in the reflectivity spectra. Notably, in (b), which corresponds to an overdamped system, parametric driving gives rise to an interesting structure from a featureless background with a dip on resonance.

phonon mode. The Hamiltonian describing such a model can be written as

$$H_{ph} = ZEQ + M\omega_{ph}^2 \frac{Q^2}{2} + \frac{\Pi^2}{2M}, \quad (33)$$

where Q is the phonon coordinate, Π is the momentum conjugate to Q , $\omega_{ph.}$ is the transverse phonon frequency, M is the ion mass, and Z is the effective charge of the phonon mode.

Solving the equations of motion corresponding to Eq. (33) together with Maxwell's equations we obtain two hybrid light-matter modes corresponding to the upper and lower polaritons. In equilibrium the dispersion and typical reflectivity is given by Figs. 2(b)–2(d). The dispersion is modeled by taking the refractive index given by Eq. (7) written here for convenience:

$$n(\omega)^2 = \epsilon_\infty \left(1 + \frac{\omega_{pl.,phonon}^2}{-\omega^2 - i\gamma\omega + \omega_{ph.}^2} \right),$$

where in terms of our Hamiltonian parameters the plasma frequency of the phonon is given by $\omega_{pl.,phonon}^2 = \frac{Z^2}{\epsilon_0 M}$. The bottom of the upper polariton branch is at frequency $\omega_L = \sqrt{\omega_{ph.}^2 + \omega_{pl.,phonon}^2}$.

A new feature of the two band system is the possibility of interband parametric resonances. The simplest type of optical pump corresponds to resonantly exciting the upper polariton branch at $k = 0$, which then results in the parametric drive of the system at frequency $\Omega_d = 2\omega_L$ [18] (for details see

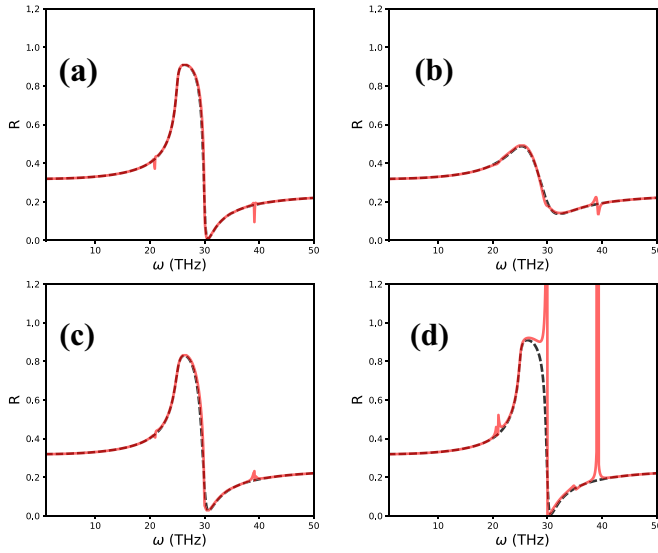


FIG. 5. Reflectivity spectra of a phonon-polariton system driven by $\Omega_d = 60$ THz through exciting the upper phonon-polariton at 30 THz. The four regimes of the phase diagram are presented for different parameters of the phonon dissipation and oscillation amplitude. The values were chosen such that the transverse phonon is at $\omega_T = 25$ THz and the longitudinal phonon is at $\omega_L = 30$ THz. (a) Regime I: $\gamma = 0.5$ THz, $B = 2.7 \times 10^7 \frac{\text{THz}^4}{c^2}$; (b) Regime II: $\gamma = 5$ THz, $B = 9 \times 10^7 \frac{\text{THz}^4}{c^2}$; (c) Regime III: $\gamma = 1$ THz, $B = 7000 \frac{\text{THz}^4}{c^2}$; (d) Regime IV: $\gamma = 0.5$ THz, $B = 8.1 \times 10^7 \frac{\text{THz}^4}{c^2}$. In Regime IV, apart from the expected parametrically resonant instabilities, we find a Fano-type feature associated with divergences in the strength of the phonon-mediated parametric drive. This occurs at $\Omega_d - \omega_T = 35$ THz.

Appendix B). This is the situation that we will primarily focus on in this section. As shown in Fig. 2(b), in this case one finds a resonant process in which the drive produces one lower and one upper polariton at finite momentum. This process satisfies both momentum and energy conservation. This resonance leads to singularities in the reflectivity shown in Fig. 5 at 20 and 40 THz. Another case of parametric resonance corresponds to the drive creating two upper polaritons at zero momentum. This leads to the singularity at $\omega_L = 30$ THz in Fig. 5(d).

Another small peak in Fig. 5(d) (strong drive regime) can be seen at the frequency of 35 THz. This feature arises from the singularity of the matrix element that mixes the signal and idler frequency components that we pointed out in Sec. IB. In Appendix B, we consider nonlinearities in the phonon system of the type

$$H_{\text{non-linear}} = uQ^4 \quad (34)$$

and demonstrate that the matrix element A_{drive} , introduced in Eq. (14), can be written as

$$A_{\text{drive}}(\omega_s) = A_{\text{drive},0} + \frac{B}{(\omega_s^2 + i\gamma\omega_s - \omega_{ph.}^2)(\omega_{id.}^2 + i\gamma\omega_{id.} - \omega_{ph.}^2)}. \quad (35)$$

The last equation shows that Floquet mixing is dramatically enhanced when either the signal or the idler frequencies are equal to $\omega_{ph.}$. It is also useful to present this result in terms of the effective change of the index of refraction (at the signal frequency) after integrating out contribution of the idler component [see Eq. (23)]. In the phonon-polariton case we obtain correction to the index of refraction

$$\delta n_{\text{phonon}} \propto \frac{1}{(\omega_{id.}^2 + i\gamma\omega_{id.} - \omega_{ph.}^2)(\omega_s^2 + i\gamma\omega_s - \omega_{ph.}^2)}, \quad (36)$$

which shows resonant enhancement around $\omega_s = \omega_{ph.}$ and $\omega_s = \Omega_d - \omega_{ph.}$. We remind the readers, however, that Eq. (36) is based on the perturbative treatment of the signal-idler mixing and is not quantitatively accurate in the vicinity of singularities in the reflection coefficient.

IV. BLUE-SHIFTED EDGE IN BILAYER HIGH T_c CUPRATE $\text{YBa}_2\text{Cu}_3\text{O}_{6.5}$

An experimental realization of the driven single plasmon edge comes from terahertz pump and probe experiments in $\text{YBa}_2\text{Cu}_3\text{O}_{6.5}$ [45]. In equilibrium, $\text{YBa}_2\text{Cu}_3\text{O}_{6.5}$ is a bilayer SC with a JP at 0.9 THz. The low-energy optical response for light polarized along the c axis of the material is captured by the equations of motion [41]:

$$\left(n_0^2(\omega^2 - \omega_{pl.}^2) + i\frac{\sigma_n}{\epsilon_0}\omega - c^2k^2 \right) E = 0, \quad (37)$$

where σ_n represents the conductivity of the normal state electron fluid which provides dissipation for the JP, $\omega_{pl.}$ is the Josephson plasma frequency, and n_0 is the static refractive index inside the material. This photon dispersion is shown in Fig. 2(a) with a gap $\omega_{JP} \sim 0.9$ THz leading to a JP edge at that frequency in the equilibrium optical reflectivity. Equivalently, the equations of motion can be represented by the refractive index:

$$n_{\text{SC}}(\omega) = n_0^2 \left(\frac{\omega^2 - \omega_{pl.}^2}{\omega^2} + i\frac{\sigma_n}{\epsilon_0 n_0^2 \omega} \right), \quad (38)$$

substituted in Eq. (4).

We use our model to fit experimental data presented in Ref. [45] (reprinted here with the author's permission). Parameters used in this section to produce the figures are tabulated in Appendix C. We consider first a low-temperature state in the superconducting regime, $T = 10$ K, and model pumping as parametrically driving JPs [21,22]. Using our simple model, we find excellent agreement with experiments shown in Fig. 6 and interpret the edge at ~ 1 THz to be a consequence of parametric resonance from a drive at ~ 2 THz, corresponding to the intermediate Regime IV in the phase diagram. To fit the data, we need to assume that the normal state conductivity, σ_n , is increased in the pumped state by photo-excited quasiparticles but also that $\omega_{pl.}^2$, which is proportional to the superfluid density, is decreased. Remarkably, our simulation shows that even if we assume a suppressed superfluid density, we still find a blue-shifted edge as a result of internal oscillating fields parametrically driving JPs. To fit the photo-induced edge above T_c , we model the pseudogap phase as a SC with overdamped dynamics and a reduced

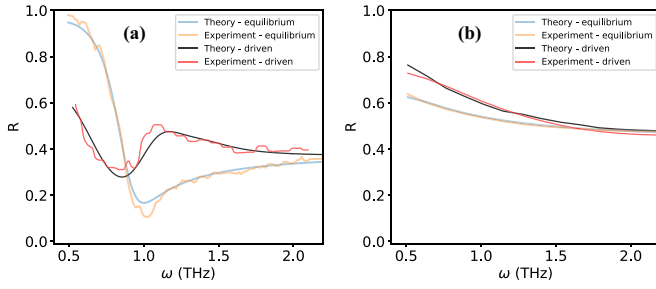


FIG. 6. Optical reflectivity spectra of $\text{YBa}_2\text{Cu}_3\text{O}_{6.5}$ extracted from Ref. [45], replotted with the permission of the authors and fitted with the theory presented in this paper. The photo-induced reflectivity edge is well captured by our simple model and suggests that JPs are parametrically driven by a coherently oscillating mode. (a) Reflectivity spectra at $T = 10$ K (below T_c) shows a dip peak structure around 1 THz corresponding to Regime (I) of our phase diagram. (b) Reflectivity spectra at $T = 100$ K (above T_c) is fitted with our theory assuming an overdamped JP edge in the pseudogap regime. Parametric driving produces changes in reflectivity consistent to Regime (II) of our phase diagram. Fitting parameters are reported in Appendix C.

plasma resonance frequency. In Fig. 6(b) we are able to fit the data assuming parametric driving at the same frequency as the low-temperature data. Our theory suggests that reflectivity data from pump and probe experiments in the pseudogap phase of $\text{YBa}_2\text{Cu}_3\text{O}_{6.5}$ correspond to Regime II of our phase diagram, which shows that a photo-induced edge appears as a result of parametric driving of overdamped photon modes.

V. DISCUSSION AND OUTLOOK

In this paper we developed a theory that allows to compute optical reflectivity of materials with oscillating collective modes. We demonstrated that by using only a few phenomenological coefficients, which parametrize the frequency-dependent refractive index, as well as the frequency of the oscillations driving the system, it is possible to predict the position of the photo-induced resonances associated with parametric resonances. To obtain the shape of the resonant feature, one also needs to include information about the amplitude of the drive and dissipation of collective modes. In particular, we found that when dissipation dominates over parametric drive, the system develops a Lorentzian-shaped dip, which arises from the interference of signal and idler transmission channels. At stronger drives the dip turns into a peak and reflectivity can exceed one, indicating parametric amplification of the probe pulse. We also discussed interesting double dip crossover behavior between the overdamped and the amplification regimes. Our results should be ubiquitous in strongly driven systems where the excitation of a well-defined collective mode can act as the external periodic drive.

Our analysis demonstrates that parametric resonances provide a general universality class of reflectivity features from which both dynamical and static properties of the system can be extracted. This puts them in the same category as previously studied Fano resonance features and EIT [35]. Despite the simplicity of our model, the resulting reflectivity spectrum can be quite rich, as shown in the phase diagram in Fig. 1. Our

results provide a tool for analyzing a variety of photo-induced features that have been observed in experiments but have not been given theoretical interpretation until now. We show that photo-induced features, such as a photo-induced edge, can serve as a reporter of a long-lived collective mode excited in the material during pumping and a precursor of a lasing instability that can occur in the system at stronger drives. As a concrete case study we analyzed experimental results of the pump-induced changes of reflectivity in a layered SC $\text{YBa}_2\text{Cu}_3\text{O}_{6.5}$ at frequencies close to the lower JP edge. We find that we can obtain an accurate fit to the experimental data if we include strong renormalization of the equilibrium parameters, such as enhancement of real conductivity due to the photoexcitation of charge carriers during the pump.

A natural generalization of the above framework is the inclusion of time-dependent drives at several frequencies. This is important, for example, for analyzing Floquet drives with finite spectral width or including finite lifetime of collective modes. In this case different oscillating modes are expected to compete with each other, leading to an inhomogeneous broadening of the dip/peak features predicted in this work.

ACKNOWLEDGMENTS

M.H.M. and E.D. acknowledge support from Harvard-MIT CUA, AFOSR-MURI: Photonic Quantum Matter (Grant No. FA95501610323), the ARO grant “Control of Many-Body States Using Strong Coherent Light-Matter Coupling in Terahertz Cavities,” and the National Science Foundation through grant NSF EAGER-QAC-QSA (Grant No. 2222-206-2014111). S.R.U.H. and R.D.A. acknowledge support from the DARPA DRINQS program (Grant No. D18AC00014). D.P. thanks support by the Israel Science Foundation (Grant No. 1803/18).

APPENDIX A: DERIVATION OF FLOQUET REFRACTIVE INDEX IN THE STABLE REGIME

In this section we derive the Floquet refractive index shown in Eq. (23). Using Eqs. (20) and (21) we derive the perturbative Floquet-Fresnel equations:

$$1 + r_s = t_s + \frac{\xi}{2} t_{id.}, \quad (\text{A1a})$$

$$1 - r_s = t_s \frac{c\tilde{k}_s}{\omega_s} + \frac{\xi}{2} \frac{c\tilde{k}_{id.}}{\omega_s}, \quad (\text{A1b})$$

$$r_{id.} = -\frac{\xi}{2} t_s + t_{id.}, \quad (\text{A1c})$$

$$r_{id.} = -\frac{\xi}{2} \frac{c\tilde{k}_s}{\omega_{id.}} t_s + \frac{c\tilde{k}_{id.}}{\omega_{id.}} t_{id.} \quad (\text{A1d})$$

We can integrate out the effects of the idler channel by using Eqs. (A1c) and (A1d): We wish to use the boundary conditions oscillating at the idler frequency to solve for $t_{id.}$ in terms of t_s :

$$t_{id.} = \frac{\xi}{2} \frac{c\tilde{k}_s - \omega_{id.}}{c\tilde{k}_{id.} - \omega_{id.}} t_s. \quad (\text{A2})$$

These lead to the boundary conditions:

$$1 + r_s = t_s \left(1 + \frac{\xi^2}{4} \frac{c\tilde{k}_s - \omega_{id.}}{c\tilde{k}_{id.} - \omega_{id.}} \right), \quad (\text{A3a})$$

$$1 - r_s = t_s \frac{c\tilde{k}_s}{\omega_s} \left(1 + \frac{\xi^2}{4} \frac{c\tilde{k}_s - \omega_{id.}}{c\tilde{k}_{id.} - \omega_{id.}} \frac{\tilde{k}_{id.}}{\tilde{k}_s} \right). \quad (\text{A3b})$$

After rescaling the transmission coefficient t_s , the above equation can be cast in the familiar form:

$$1 + r_s = t_s, \quad (\text{A4a})$$

$$1 - r_s = t_s \tilde{n}, \quad (\text{A4b})$$

allowing us to encode the effects of driving into an effective renormalized refractive index. In fact, the possibility for the dressed refractive index to be negative is what gives rise to phenomena such as parametric amplification of reflectivity. The renormalized refractive index is found to be:

$$\tilde{n} \approx \frac{c\tilde{k}_s}{\omega_s} \frac{1 + \frac{\xi^2}{4} \frac{c\tilde{k}_s - \omega_{id.}}{c\tilde{k}_{id.} - \omega_{id.}} \cdot \frac{\tilde{k}_{id.}}{\tilde{k}_s}}{1 + \frac{\xi^2}{4} \frac{c\tilde{k}_s - \omega_{id.}}{c\tilde{k}_{id.} - \omega_{id.}}}, \quad (\text{A5a})$$

$$\tilde{n} \approx n_{eq.} \left(1 + \frac{A_{drive}\xi}{4k_s^2} + \frac{\xi^2}{4} \frac{c\tilde{k}_s - \omega_{id.}}{c\tilde{k}_{id.} - \omega_{id.}} \left(\frac{\tilde{k}_{id.}}{\tilde{k}_s} - 1 \right) \right) \quad (\text{A5b})$$

as reported in Eq. (23).

APPENDIX B: IR PHONON-MEDIATED DRIVE

The equation of motion for the phonon given by the Hamiltonian in Eqs. (33) and (34) is

$$(\partial_t^2 + \gamma \partial_t + \omega_0^2 + 4uQ^2)Q = ZE. \quad (\text{B1})$$

Using a Gaussian ansatz for the phonons we can linearize the above equation as:

$$(\partial_t^2 + \gamma \partial_t + \omega_{ph.}^2 + 12u\langle Q^2 \rangle)Q = \frac{Z}{M}E. \quad (\text{B2})$$

The phonon mode appears in the Maxwells equations as:

$$\left(\frac{1}{c^2} \partial_t^2 - k^2 \right) E = -Z \partial_t^2 Q. \quad (\text{B3})$$

Oscillating collective modes inside the material will affect the above linear system through oscillations of $\langle Q^2 \rangle = \langle X^2 \rangle_0 + A(e^{i\Omega_d t} + e^{-i\Omega_d t})$. Such a term can arise by pumping the system on resonance with the upper polariton, such that $\langle Q \rangle = A' \cos \omega_L t$, where $\omega_L^2 = \omega_{ph.}^2 + \frac{Z^2}{M}$, the frequency of the upper polariton at $k = 0$. Alternatively, for a pumping protocol at high frequencies, the upper polariton fluctuations, $\langle Q^2 \rangle$, can be driven linearly by a Raman process. In both cases, the driving frequency would be twice the upper plasmon frequency $\Omega_d = 2\omega_L$. However, in general, Ω_d can also correspond to a different frequency not included in our model. Absorbing $\langle Q^2 \rangle_0$ in the definition of $\omega_{ph.}$ and expanding in Eq. (B2) Q in signal and idler components, $Q = Q_s e^{-i\omega_s t} + Q_{id.} e^{i\omega_{id.} t}$ we have

$$\begin{pmatrix} Q_s \\ Q_{id.} \end{pmatrix} = \begin{pmatrix} \frac{Z}{\omega_s^2 + i\gamma\omega_s - \omega_{ph.}^2} & 0 \\ 0 & \frac{Z}{\omega_{id.}^2 + i\gamma\omega_{id.} - \omega_{ph.}^2} \end{pmatrix} \cdot \begin{pmatrix} E_s \\ E_{id.} \end{pmatrix} + \frac{ZA}{(\omega^2 + i\gamma\omega - \omega_{ph.}^2)(\omega_{id.}^2 + i\gamma\omega_{id.} - \omega_{ph.}^2)} \begin{pmatrix} E_{id.} \\ E_s \end{pmatrix}. \quad (\text{B4})$$

Substituting Eq. (B4) in Maxwell's equation we find the equations of motion for the signal and idler component to be:

$$\left(\frac{n_{eq.}^2(\omega_s)}{c^2} \omega_s^2 - k^2 \right) E_s + A_{drive,s}(\omega_s, \omega_{id.}) E_{id.} = 0, \quad (\text{B5a})$$

$$\left(\frac{n_{eq.}^2(\omega_{id.})}{c^2} \omega_{id.}^2 - k^2 \right) E_{id.} + A_{drive,id}(\omega_s, \omega_{id.}) E_s = 0, \quad (\text{B5b})$$

where the signal and idler driving amplitude, $A_{drive,s}$ and $A_{drive,id}$ is given by:

$$A_{drive,s} = \frac{Z^2 A \omega_s^2}{(\omega^2 + i\gamma\omega - \omega_{ph.}^2)(\omega_{id.}^2 + i\gamma\omega_{id.} - \omega_{ph.}^2)}, \quad (\text{B6a})$$

$$A_{drive,id} = \frac{Z^2 A \omega_{id.}^2}{(\omega^2 + i\gamma\omega - \omega_{ph.}^2)(\omega_{id.}^2 + i\gamma\omega_{id.} - \omega_{ph.}^2)}, \quad (\text{B6b})$$

justifying the resonant structure presented in Eq. (35).

APPENDIX C: FITTING PARAMETERS FOR $\text{YBa}_2\text{Cu}_3\text{O}_{6.5}$ DATA

As mentioned, equilibrium is modeled via the equations of motion of photons in a SC:

$$\left(\omega^2 + i \frac{\sigma_n}{\epsilon_0} \omega - \left(\omega_{pl.}^2 + \frac{c^2}{n^2} k^2 \right) \right) E(\omega) = 0. \quad (\text{C1})$$

Driving is taken into account by mixing signal and idler frequency contributions arising from a periodic drive at Ω_d :

$$\left(\omega_s^2 + i \frac{\sigma_n}{\epsilon_0} \omega_s - \left(\omega_{pl.}^2 + \frac{c^2}{n^2} k^2 \right) \right) E(\omega_s, k) + A_{drive} E(-\omega_{id.}, k) = 0, \quad (\text{C2a})$$

$$\left(\omega_{id.}^2 + i \frac{\sigma_n}{\epsilon_0} \omega_{id.} - \left(\omega_{pl.}^2 + \frac{c^2}{n^2} k^2 \right) \right) E(-\omega_{id.}, k) + A_{drive} E(\omega_s, k) = 0. \quad (\text{C2b})$$

To fit the data, we first fit the parameters $\{\omega_{pl}, \sigma_n, n\}$ to the equilibrium reflectivity and then fit the driving frequency Ω_d and driving amplitude A_{drive} to match the driven reflectivity spectra.

1. Below T_c

The experimental data taken at 10 K, with pumping frequency of 19.2 THz with a width of 1 THz and electric-field amplitude 1 MV/cm. The equilibrium is fitted with $\omega_{pl} = 0.9$ THz, $\sigma/\epsilon_0 = 2.7$ THz, $n = 4.2$. In the driven state we use $\Omega_d = 2.1$ THz, $A_{\text{drive}} = 8.4 \frac{\text{THz}^2}{c^2}$, $\omega_{pl} = 0.6$ THz and $\sigma_n/\epsilon_0 = 5.5$ THz. From our fit we predict that dissipation has increased due to pumping but also the interlayer Josephson coupling has

decreased during the pump. We see that the edge appears even if the Josephson coupling is suppressed.

2. Above T_c

The experimental data taken at 10 K, with pumping frequency of 19.2 THz with a width of 1 THz and electric-field amplitude 3 MV/cm. Equilibrium is found to be overdamped with $\omega_{pl} = 0.1$ THz, $\sigma/\epsilon_0 = 25.8$ THz, $n = 5$. The pumped reflectivity is fitted with $\Omega_d = 3.8$ THz, $A_{\text{drive}} = 64 \frac{\text{THz}^2}{c^2}$, $\omega_{pl} = 0.1$ THz and $\sigma_n/\epsilon_0 = 54$ THz.

Finally, both signals were convoluted with a Gaussian broadening function, with standard deviation 0.05 THz.

-
- [1] H. Aoki, N. Tsuji, M. Eckstein, M. Kollar, T. Oka, and P. Werner, Nonequilibrium dynamical mean-field theory and its applications, *Rev. Mod. Phys.* **86**, 779 (2014).
 - [2] A. de la Torre, D. M. Kennes, M. Claassen, S. Gerber, J. W. McIver, and M. A. Sentef, *Colloquium: Nonthermal pathways to ultrafast control in quantum materials*, *Rev. Mod. Phys.* **93**, 041002 (2021).
 - [3] D. Fausti, R. I. Tobey, N. Dean, S. Kaiser, A. Dienst, M. C. Hoffmann, S. Pyon, T. Takayama, H. Takagi, and A. Cavalleri, Light-induced superconductivity in a stripe-ordered cuprate, *Science* **331**, 189 (2011).
 - [4] D. Nicoletti, E. Casandruc, Y. Laplace, V. Khanna, C. R. Hunt, S. Kaiser, S. S. Dhesi, G. D. Gu, J. P. Hill, and A. Cavalleri, Optically induced superconductivity in striped $\text{La}_{2-x}\text{Ba}_x\text{CuO}_4$ by polarization-selective excitation in the near infrared, *Phys. Rev. B* **90**, 100503(R) (2014).
 - [5] W. Hu, S. Kaiser, D. Nicoletti, C. R. Hunt, I. Gierz, M. C. Hoffmann, M. L. Tacon, T. Loew, B. Keimer, and A. Cavalleri, Optically enhanced coherent transport in $\text{YBa}_2\text{Cu}_3\text{O}_{6.5}$ by ultrafast redistribution of interlayer coupling, *Nat. Mater.* **13**, 705 (2014).
 - [6] Jun-ichi Okamoto, A. Cavalleri, and L. Mathey, Theory of Enhanced Interlayer Tunneling in Optically Driven High- T_c Superconductors, *Phys. Rev. Lett.* **117**, 227001 (2016).
 - [7] J. Zhang, X. Tan, M. Liu, S. W. Teitelbaum, K. W. Post, F. Jin, K. A. Nelson, D. N. Basov, W. Wu, and R. D. Averitt, Cooperative photoinduced metastable phase control in strained manganite films, *Nat. Mater.* **15**, 956 (2016).
 - [8] L. Stojchevska, I. Vaskivskiy, T. Mertelj, P. Kusar, D. Svetin, S. Brazovskii, and D. Mihailovic, Ultrafast switching to a stable hidden quantum state in an electronic crystal, *Science* **344**, 177 (2014).
 - [9] Y. H. Wang, H. Steinberg, P. Jarillo-Herrero, and N. Gedik, Observation of floquet-bloch states on the surface of a topological insulator, *Science* **342**, 453 (2013).
 - [10] E. J. Sie, C. M. Nyby, C. D. Pemmaraju, S. J. Park, X. Shen, J. Yang, M. C. Hoffmann, B. K. Ofori-Okai, R. Li, A. H. Reid, S. Weathersby, E. Mannebach, N. Finney, D. Rhodes, D. Chenet, A. Antony, L. Balicas, J. Hone, T. P. Devereaux, T. F. Heinz *et al.*, An ultrafast symmetry switch in a weyl semimetal, *Nature (London)* **565**, 61 (2019).
 - [11] J. W. McIver, B. Schulte, F.-U. Stein, T. Matsuyama, G. Jotzu, G. Meier, and A. Cavalleri, Light-induced anomalous Hall effect in graphene, *Nat. Phys.* **16**, 38 (2020).
 - [12] D. N. Basov, R. D. Averitt, D. van der Marel, M. Dressel, and K. Haule, Electrodynamics of correlated electron materials, *Rev. Mod. Phys.* **83**, 471 (2011).
 - [13] P. E. Dolgirev, M. H. Michael, J. B. Curtis, D. Nicoletti, M. Buzzi, M. Fechner, A. Cavalleri, and E. Demler, Theory for anomalous terahertz emission in striped cuprate superconductors (2021), [arXiv:2112.05772](https://arxiv.org/abs/2112.05772) [cond-mat.supr-con].
 - [14] P. E. Dolgirev, A. Zong, M. H. Michael, J. B. Curtis, D. Podolsky, A. Cavalleri, and E. Demler, Periodic dynamics in superconductors induced by an impulsive optical quench (2022), [arXiv:2104.07181](https://arxiv.org/abs/2104.07181) [cond-mat.supr-con].
 - [15] D. N. Basov, R. D. Averitt, and D. Hsieh, Towards properties on demand in quantum materials, *Nat. Mater.* **16**, 1077 (2017).
 - [16] Z. Sun and A. J. Millis, Bardasis-Schrieffer polaritons in excitonic insulators, *Phys. Rev. B* **102**, 041110(R) (2020).
 - [17] K. A. Cremin, J. Zhang, C. C. Homes, G. D. Gu, Z. Sun, M. M. Fogler, A. J. Millis, D. N. Basov, and R. D. Averitt, Photoenhanced metastable c-axis electrodynamics in stripe-ordered cuprate $\text{La}_{1.885}\text{Ba}_{0.115}\text{CuO}_4$, *Proc. Natl. Acad. Sci. U.S.A.* **116**, 19875 (2019), <https://www.pnas.org/content/116/40/19875.full.pdf>.
 - [18] A. Cartella, T. F. Nova, M. Fechner, R. Merlin, and A. Cavalleri, Parametric amplification of optical phonons, *Proc. Natl. Acad. Sci. U.S.A.* **115**, 12148 (2018), <https://www.pnas.org/content/115/48/12148.full.pdf>.
 - [19] M. Budden, T. Gebert, M. Buzzi, G. Jotzu, E. Wang, T. Matsuyama, G. Meier, Y. Laplace, D. Pontiroli, M. Ricc , F. Schlawin, D. Jaksch, and A. Cavalleri, Evidence for metastable photo-induced superconductivity in K_3C_{60} , *Nat. Phys.* **17**, 611 (2021).
 - [20] M. Buzzi, G. Jotzu, A. Cavalleri, J. I. Cirac, E. A. Demler, B. I. Halperin, M. D. Lukin, T. Shi, Y. Wang, and D. Podolsky, Higgs-Mediated Optical Amplification in a Nonequilibrium Superconductor, *Phys. Rev. X* **11**, 011055 (2021).
 - [21] A. von Hoegen, M. Fechner, M. F rst, N. Taherian, E. Rowe, A. Ribak, J. Porras, B. Keimer, M. Michael, E. Demler, and A. Cavalleri, Parametrically amplified phase-incoherent

- superconductivity in $\text{YBa}_2\text{Cu}_3\text{O}_{6+x}$ (2020), [arXiv:1911.08284](#) [cond-mat.supr-con].
- [22] M. H. Michael, A. von Hoegen, M. Fechner, M. Först, A. Cavalleri, and E. Demler, Parametric resonance of josephson plasma waves: A theory for optically amplified interlayer superconductivity in $\text{YBa}_2\text{Cu}_3\text{O}_{6+x}$, *Phys. Rev. B* **102**, 174505 (2020).
- [23] R. Shimano and N. Tsuji, Higgs mode in superconductors, *Annu. Rev. Condens. Matter Phys.* **11**, 103 (2020).
- [24] F. Giorgianni, T. Cea, C. Vicario, C. P. Hauri, W. K. Withanage, X. Xi, and L. Benfatto, Leggett mode controlled by light pulses, *Nat. Phys.* **15**, 341 (2019).
- [25] F. Gabriele, M. Udina, and L. Benfatto, Non-linear terahertz driving of plasma waves in layered cuprates, *Nat. Commun.* **12**, 752 (2021).
- [26] S. J. Denny, S. R. Clark, Y. Laplace, A. Cavalleri, and D. Jaksch, Proposed Parametric Cooling of Bilayer Cuprate Superconductors by Terahertz Excitation, *Phys. Rev. Lett.* **114**, 137001 (2015).
- [27] S. Rajasekaran, E. Casandruc, Y. Laplace, D. Nicoletti, G. D. Gu, S. R. Clark, D. Jaksch, and A. Cavalleri, Parametric amplification of a superconducting plasma wave, *Nat. Phys.* **12**, 1012 (2016).
- [28] A. Dienst, E. Casandruc, D. Fausti, L. Zhang, M. Eckstein, M. Hoffmann, V. Khanna, N. Dean, M. Gensch, S. Winnerl, W. Seidel, S. Pyon, T. Takayama, H. Takagi, and A. Cavalleri, Optical excitation of josephson plasma solitons in a cuprate superconductor, *Nat. Mater.* **12**, 535 (2013).
- [29] S. Rajasekaran, J. Okamoto, L. Mathey, M. Fechner, V. Thampy, G. D. Gu, and A. Cavalleri, Probing optically silent superfluid stripes in cuprates, *Science* **359**, 575 (2018).
- [30] F. Schmitt, P. S. Kirchmann, U. Bovensiepen, R. G. Moore, J.-H. Chu, D. H. Lu, L. Rettig, M. Wolf, I. R. Fisher, and Z.-X. Shen, Ultrafast electron dynamics in the charge density wave material TbTe_3 , *New J. Phys.* **13**, 063022 (2011).
- [31] R. W. Boyd, *Nonlinear Optics, Third Edition* (Academic Press, New York, 2008).
- [32] L. Broers and L. Mathey, Observing light-induced floquet band gaps in the longitudinal conductivity of graphene, [arXiv:2103.01949](#) (2021).
- [33] G. Homann, J. G. Cosme, and L. Mathey, Terahertz amplifiers based on gain reflectivity in cuprate superconductors, *Phys. Rev. Res.* **4**, 013181 (2022).
- [34] S. E. Harris, G. Y. Yin, A. Kasapi, M. Jain, and Z. F. Luo, Electromagnetically induced transparency, in *Coherence and Quantum Optics VII*, edited by J. H. Eberly, L. Mandel, and E. Wolf (Springer, Boston, MA, 1996), pp. 295–304.
- [35] M. F. Limonov, M. V. Rybin, A. N. Poddubny, and Y. S. Kivshar, Fano resonances in photonics, *Nat. Photonics* **11**, 543 (2017).
- [36] A. Eckardt and E. Anisimovas, High - frequency approximation for periodically driven quantum systems from a floquet - space perspective, *New J. Phys.* **17**, 093039 (2015).
- [37] S. Sugiura, E. A. Demler, M. Lukin, and D. Podolsky, Resonantly enhanced polariton wave mixing and floquet parametric instability, [arXiv:1910.03582](#) (2019).
- [38] P. Dolgirev, M. H. Michael, and E. Demler, Multi-tonal floquet-fresnel equations (unpublished).
- [39] R. A. Fisher, *Optical Phase Conjugation* (Academic Press, San Diego, 1983).
- [40] B. Zel'Dovich, N. Pilipetsky, and V. Shkunov, *Principles of Phase Conjugation*, Springer Series in Optical Sciences (Springer-Verlag, Berlin, Heidelberg, Heidelberg, 1985).
- [41] M. Tinkham, *Introduction to Superconductivity* (Dover Publications, Mineola, New York, 2004).
- [42] F. Wooten, Chapter 2 - Maxwell's equations and the dielectric function, in *Optical Properties of Solids*, edited by F. Wooten (Academic Press, New York, 1972), pp. 15–41.
- [43] A. Roy and M. Devoret, Introduction to parametric amplification of quantum signals with josephson circuits, *C. R. Phys.* **17**, 740 (2016), quantum microwaves/Micro-ondes quantiques.
- [44] L. N. Bulaevskii, M. Zamora, D. Baeriswyl, H. Beck, and J. R. Clem, Time-dependent equations for phase differences and a collective mode in Josephson-coupled layered superconductors, *Phys. Rev. B* **50**, 12831 (1994).
- [45] B. Liu, M. Först, M. Fechner, D. Nicoletti, J. Porras, T. Loew, B. Keimer, and A. Cavalleri, Pump Frequency Resonances for Light-Induced Incipient Superconductivity in $\text{YBa}_2\text{Cu}_3\text{O}_{6.5}$, *Phys. Rev. X* **10**, 011053 (2020).